A Novel Solar Simulator Based on a Supercontinuum Laser for Solar Cell Device and Materials Characterization

Tasshi Dennis, John B. Schlager, *Senior Member, IEEE*, and Kris A. Bertness, *Senior Member, IEEE*

***Abstract*—The design, operation, and application of a novel solar simulator based on a high-power supercontinuum fiber laser are described. The simulator features a multisun irradiance with continuous spectral coverage from the visible to the infrared. By use of a prism-based spectral shaper, the simulator can be matched to any desired spectral profile, including the ASTM G-173-03 air-mass 1.5 reference spectrum. The simulator was used to measure the efficiency of gallium arsenide (GaAs), crystalline silicon (Si), amorphous Si, and copper–indium–gallium–selenide (CIGS) thin-film solar cells, showing agreement with independent measurements. The pulsed temporal characteristic of the simulator was studied and would appear to have a negligible influence on measured cell efficiency. The simulator light was focused to a spot of approximately 8 μm in diameter and used to create micrometer-scale spatial maps of full spectrum optical-beam-induced current. Microscopic details such as grid lines, damage spots, and material variations were selectively excited and resolved on GaAs and CIGS cells. The spectral shaping capabilities were used to create output spectra appropriate for selectively light-biasing multijunction cell layers. The simulator was used to create variable blue-rich and red-rich spectra that were applied to a GaInP/GaAs tandem solar cell to illustrate the current-limiting behavior.**

***Index Terms*—External quantum efficiency (EQE), metrology, microscopy, multijunction, optical-beam-induced current, photovoltaic, responsivity, solar cell, solar simulator, spectral mismatch, supercontinuum laser.**

I. Introduction

FURTHER improvements to the efficiency of solar cells for all materials and technologies depend critically on a better understanding of their optical and electrical characteristics. The study of defects caused by impurities or crystalline grain boundaries, artifacts from deposition and growth processes, and third-generation materials having microarrays or structured conduction paths could all potentially benefit from a solar simulator offering a diffraction-limited focus. In addition, the characterization of multijunction materials could benefit from selective light biasing of the different junctions made possible by a source with an accurately shaped spectrum delivered by a single collimated beam [1]. Solar simulators are typically based on lamps, such as the xenon arc-lamp [2], or arrays of light-emitting diodes [3], [4]. However, it is challenging to efficiently apply these light sources to measurement systems that require focused and/or spectrally shaped light. Fundamentally, bulb-based and point light sources typically radiate into large solid angles, thereby generating a low number of photons for any single spatial mode. This low spatial coherence makes it difficult if not impossible to efficiently use optical beam processing to achieve diffraction-limited focusing and/or arbitrary spectral shaping.

Recently, high-power supercontinuum lasers that offer spectral coverage from the visible (blue) out to the infrared have become commercially available [5]. These white-light lasers rely on optical-fiber amplifier technology to raise the peak power of a seed laser to around 100 kW per pulse. Launching these amplified pulses into a photonic crystal fiber results in the broadening of the spectrum of the seed laser through nonlinear optical mixing. The nonlinear interactions are enabled by the unique propagation characteristics of the photonic crystal fiber, which include a single spatial mode and a flat chromatic dispersion profile across the entire low-loss window of silica from about 400 to 2200 nm. The single mode creates a tight confinement of optical power, and the flat dispersion allows phase-matching over a broad wavelength range. As a result, a broad spectrum containing watts of optical power can be generated within the single spatial mode, enabling diffraction-limited free-space beam propagation. However, unlike a flashed arc lamp that is pulsed with a millisecond period, the supercontinuum laser emits a train of subnanosecond pulses with a repetition rate at megahertz frequencies. A primary concern when considering these novel sources for solar simulation is whether the devices and materials being investigated will respond as if being illuminated by continuous sunlight.

In this study, we report on the use of a supercontinuum laser as a solar simulator and demonstrate the characterization of photovoltaic devices and materials. After shaping the spectrum of the laser, we measure the efficiency of a variety of sample solar cells and examine whether the temporal characteristics of the light influence the measured efficiency. We report on the application of our focused simulator to the microscopic generation of photocurrent and present spatial maps of full-spectrum optical-beam-induced current (FS-OBIC) from sample solar cells. The ability to arbitrarily spectrally shape the simulator was utilized to create light-biasing spectra for the characterization of a tandem cell with top-junction current-limiting behavior.

II. Simulator Design

To construct our simulator, we used a commercially available supercontinuum laser having more than 8 W of emission and a

Manuscript received November 27, 2013; revised April 10, 2014 and February 20, 2014; accepted February 6, 2014. Date of publication May 26, 2014; date of current version June 18, 2014. This papers constitutes work of the U.S. government and is not subject to copyright.

The authors are with the National Institute of Standards and Technology, Boulder, CO 80305 USA (e-mail: tasshi@nist.gov; john.schlager@nist.gov; bertness@boulder.nist.gov).

Color versions of one or more of the figures in this paper are available online at http://ieeexplore.ieee.org.

Digital Object Identifier 10.1109/JPHOTOV.2014.2321659

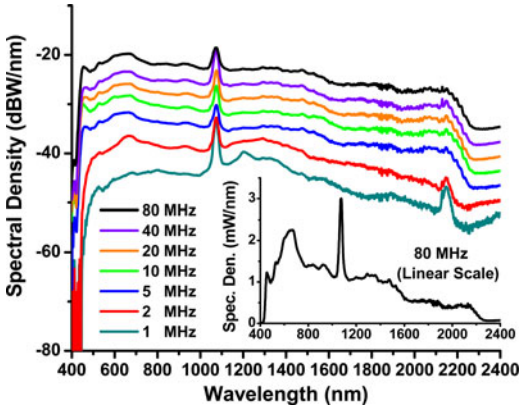

Fig. 1. Supercontinuum spectra generated at various repetition rates. Inset: 80-MHz spectrum on a linear scale.

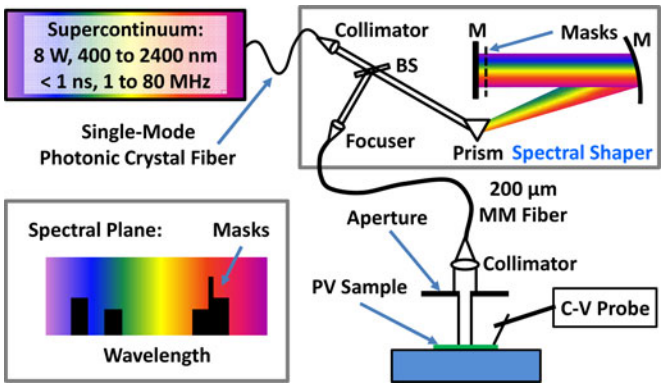

Fig. 2. Simulator system, including the mask geometry and sample illumination. M: mirror; BS: beamsplitter.

spectrum that spanned from below 450 nm to beyond 2200 nm. The laser can operate at a selectable repetition rate between 1 and 80 MHz, with the output power scaling linearly with rate, as shown on a logarithmic scale in Fig. 1. At 1 MHz, the total emission was less than 200 mW, and the visible content was weak. However, the inset of Fig. 1 shows the 80-MHz spectrum on a linear scale and demonstrates that at this repetition rate, the light content in the visible wavelength range dominates. The output emission of the supercontinuum has a single mode Gaussian beam profile, which can be collimated, shaped, or focused with conventional optics.

Our strategy for spectrally shaping the source was to use a prism-based dispersive spectrometer that was similar in design to a femtosecond pulse shaper [6] and the NIST hyperspectral image projector [7]. The output from the photonic crystal fiber was collimated by a lens and was directed onto a prism, as shown in Fig. 2. The highly dispersive prism of F2 glass was used to spread the beam across a collimation mirror having a focal length of 500 mm. The spectral beam was then directed onto a planar mirror located at the focal point of the collimation mirror to achieve maximum spectral resolution. Not shown in Fig. 2 is a cylindrical lens before the prism, which expanded the beam out of the plane of the page. In contrast with

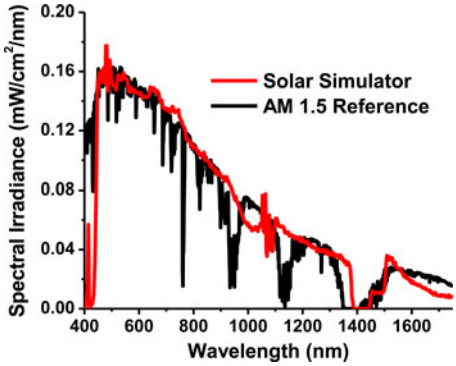

Fig. 3. Spectral shaping of the 80-MHz supercontinuum to match an AM 1.5 reference spectrum.

a line focus, this expanded beam in the spectral plane allowed varying amounts of light to be attenuated at any given wavelength by static amplitude masks. The planar mirror then returned the light back to the prism, where it was reshaped into a 10-mm diameter spatial beam. For broad-area full illumination of sample solar cells, the beam was focused into a multimode fiber with a 200-μm core, as shown in Fig. 2. Broadband parabolic reflectors were used to focus and collimate the light in and out of the multimode fiber. As we will describe later, a slightly different setup was used to create a focused spot for FS-OBIC.

Fig. 3 shows the measured irradiance spectrum of the simulator operating at 80 MHz after spectral shaping to match the air-mass (AM) 1.5 reference spectrum (ASTM G-173-03) [8]. Visually, the spectral match is quite good, with a profile that lacks the sharp resonance features of xenon-lamp simulators [9]. The integrated irradiance is 91.4 mW/cm^2 as shown, whereas AM 1.5 is 94.1 mW/cm^2. The spectral match below 450 nm is poor because the continuum generates very little light in this region. This could be a concern for the illumination of some types of cells, including multijunctions. Excluding the 400–500-nm band, the simulator easily meets the IEC 60904-9 Edition 2 (2007) standard for a class A spectral match and could be made fully compliant with less mask attenuation in the 450–500-nm band. Alternatively, several high-power light-emitting diodes may be able to supplement the short-wavelength content. The simulator can produce more than 7 suns of irradiance over a 1-cm^2 area, with a temporal stability lasting hours at a time after an initial warm-up period.

III. Solar Cell Efficiency Measurements

For the supercontinuum simulator to be a useful metrology tool, it must produce the same illuminated response in photovoltaic materials as the sun or more traditional lamp-based simulators. To gain insight, we measured the power efficiency of solar cells that had been independently characterized with lamp-based simulators. These independent characterizations were not certified calibrations and may have contributed significant uncertainties, but were sufficient for the preliminary demonstration of our novel simulator. Although expedient and promising, this effort did not constitute a formal intercomparison of laboratory

TABLE I
CELL EFFICIENCY MEASUREMENTS

	*J*sc (mA/cm^2)	*V*oc (V)	Fill Factor (%)	Eff. (%)
GaAs Cell:				
NREL	17.7	1.001	85.7	15.2
NIST 1	14.1	0.987	82.3	11.5
NIST 2	17.7	0.996	82.5	14.5
c-Si Cell:				
NREL	32.7	0.604	78.9	15.6
NIST 1	31.1	0.576	78.1	14.0
NIST 2	32.7	0.578	78.4	14.8
CIGS Cell 1:				
NREL	30.7	0.733	78.5	17.7
NIST 2	30.7	0.735	78.6	17.7
CIGS Cell 2:				
NREL	20.5	0.680	59.6	8.3
NIST 2	20.5	0.679	60.9	8.5
a-Si Cell 1:	**(A = 0.05 cm^2)**			
NREL	18.3	0.855	62.3	9.8
NIST 2	18.1	0.831	58.3	8.8
a-Si Cell 2:	**(A = 1.0 cm^2)**			
NREL	17.6	0.857	59.1	8.9
NIST 2	17.6	0.812	56.7	8.1

measurement methods. Our first-order assumption was that the response of the cells was linear and independent of wavelength, such that photons of different but sufficient energy may be exchanged to compensate for spectral mismatch [9].

Four different solar cell samples provided by the National Renewable Energy Laboratory (NREL) were used in our measurements. One was an n-GaInP/p-GaAs heterojunction cell with a total area of 0.29 cm^2 [10]. The second cell was a crystalline silicon (c-Si) device with a phosphorus-diffused emitter, full-area Al-BSF, p-type Czochralski (1 0 0) structure with an area of about 1 cm^2. The third sample was amorphous silicon (a-Si) with a p–i–n a–Si:H structure on glass utilizing through-substrate illumination and cell areas of either 0.05 or 1.0 cm^2. The fourth device was a thin-film copper–indium–gallium–selenide (CIGS) cell with an area of 0.42 cm^2.

The spectrally shaped 80-MHz output of our simulator was collimated into a Gaussian-like beam (10-mm diameter), and the central portion was masked with apertures to create a carefully controlled irradiance or to match the active areas of the cells. No aperture was used for the through-substrate illumination of the a-Si cells. The spatial nonuniformity of the beam irradiance after a 0.29-cm^2 square aperture was measured using a scanning pinhole and found to be about 25% and smoothly varying. The total optical power through the apertures was measured with a thermal power sensor and was adjusted to give a 1-sun irradiance of 100 mW/cm^2.

The first set of measured characteristics for the GaAs and c–Si cells is given in Table I as "NIST 1" and compared with independent, but not certified, conventional measurements performed at the NREL using lamp-based simulators. We estimate that the repeatability for the NIST measurements was on the order of 1% efficiency using commercial current–voltage measurement equipment,[1] whereas the absolute uncertainty was likely higher. The agreement of the results is promising and indicates that the simulator appears to be sun-like for GaAs and c-Si materials. While the short-circuit current $J_{\rm sc}$ for GaAs has a discrepancy of 20% with the NREL value, the c-Si value is within 5%. There are a number of possible explanations for the apparent discrepancies, beginning with the challenge of measuring absolute efficiencies without using a reference cell. By setting the total irradiance independent of wavelength, the results become subject to spectral mismatch [9]. In particular, the inherent lack of light below 450 nm, coupled with spectral mismatch at wavelengths above the material responsivity, may have biased the irradiance setting. It is likely that less than 1 sun of photons of sufficient energy were actually delivered to the cells. This would have influenced the GaAs cell more with its higher bandgap energy and narrower quantum efficiency bandwidth.

In the second set of measurements, we treated these same devices as reference cells and adjusted the simulator irradiance to give $J_{\rm sc}$ specified by the NREL. The measured efficiencies for this illumination are presented in Table I as "NIST 2." For both GaAs and c-Si cells, the open-circuit voltage $V_{\rm oc}$ and efficiency increased to agree more closely with the NREL values. Unfortunately, the measured fill factor for the GaAs cell was still low. Subsequent measurements performed at NIST with a class AAB xenon simulator also gave a low fill factor. Microscopic inspection of the GaAs cell revealed that many of the 100-μm-wide grid lines had been damaged in the process of contacting. Xenon simulator measurements on different GaAs cells with intact grid lines gave fill factors that agreed to $\sim$1% with NREL measurements. For the c-Si cell, only about 30% of the active area was illuminated for the results in Table I because of the small square aperture placed in the beam of the simulator. However, by removing the aperture and expanding the beam to achieve full illumination, the measured $V_{\rm oc}$ for the c-Si cell agreed to better than 1%. Subsequent measurements by NIST with the conventional xenon simulator confirmed the $V_{\rm oc}$ dependence on illumination area observed with the supercontinuum simulator. The temperatures of these cells were not tightly controlled, which also could have affected $V_{\rm oc}$. Finally, while the delivery of simulator light with the multimode fiber was convenient, it suffered from some bend loss that may have altered the spectrum of the light incident on the cells.

The measurements presented in the lower part of Table I for CIGS and a-Si cells are all labeled as "NIST 2" because the method of treating the cells as reference cells was used to set the simulator irradiance. The agreement in the efficiencies measured by NIST and NREL is especially good for the CIGS cells. The CIGS devices from the NREL do not respond to spectral content below 490 nm, which makes them less sensitive to the missing spectral content of the simulator below 450 nm. The NIST measurements of the a-Si cells are all slightly lower than the NREL values. At this time, we suspect that this may be the result of poor electrical contacting, in which hard tungsten

[1]Keithley 2401 SourceMeter; product names are only used in the paper for clarity and do not represent an endorsement by NIST.

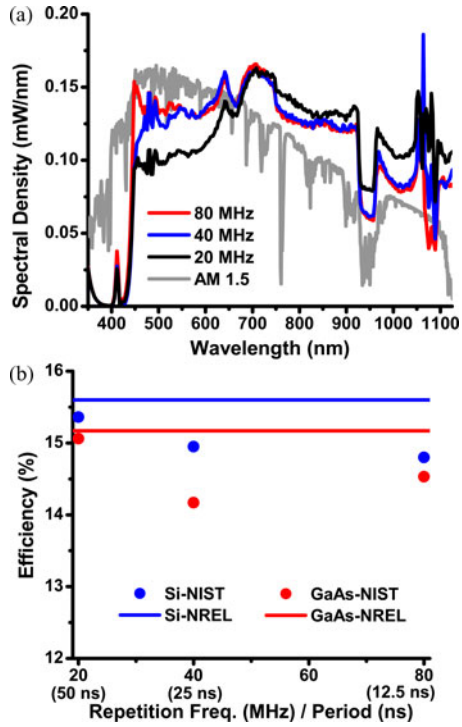

Fig. 4. Supercontinuum simulator spectra created for temporal testing (a) and the measured efficiencies (b). It should be noted that the vertical scale in (b) starts at 12 % efficiency to provide more detail for the comparison.

probe tips were used to contact the slippery back surface of the superstrate device. In addition, the back-contact geometry did not allow for convenient masking of the beam to match the cell areas. It should be noted that the NREL measurements of the a-Si cells were performed with a quartz-lamp simulator and had an estimated uncertainty of about 10%.

The supercontinuum simulator is a rapidly pulsed light source, and various cell materials may respond differently depending on their temporal characteristics. Therefore, we tested the GaAs and c-Si cells at different pulse repetition rates to check for inconsistencies. We adjusted the total irradiance of the spectrally shaped 80-MHz spectrum to give the specified $J_{\rm sc}$. However, as shown in Fig. 1, the laser output power and spectrum vary significantly with repetition rate. To avoid making unique spectral masks for each repetition rate, the total optical power from photons with energy above each cell's bandgap energy was kept constant at the repetition rates utilized below 80 MHz. The available power limited testing at 1-sun irradiance to repetition rates of 20, 40, and 80 MHz. These rates correspond to pulse periods of 50, 25, and 12.5 ns, respectively.

Fig. 4(a) shows the spectra generated for temporal testing of the c-Si cell plotted out to a wavelength of 1125 nm, which corresponds to a bandgap energy of 1.1 eV. The AM 1.5 reference spectrum is also shown, with arbitrary vertical scaling. The spectral match of the 80-MHz spectrum to AM 1.5 is not as good as that shown in Fig. 3 and was the result of some permanent spectral changes experienced by our supercontinuum laser. In addition, it is apparent that the spectral content at short wavelengths further decreases at lower repetition rates, requiring more power above 650 nm to compensate. Not shown is a similar set of spectra generated for the GaAs cell, which was analyzed out to 872 nm (1.42 eV) for equivalent total power.

A summary of the measured efficiencies is shown in Fig. 4(b), where the vertical scale starts at 12% to allow the comparison to be made in more detail. The estimated repeatability for the NIST measurements is on the order of 1% efficiency. The NREL measurements were performed with lamp-based simulators that provided continuous-wave illumination. The correspondence with the NREL efficiencies is quite good considering the technical challenges involved in making these measurements. The agreement at all repetition rates indicates that the effect of the pulsed nature of the simulator would appear to be negligible over a range of pulse periods from 12.5 to 50 ns for these two materials. Minority carrier lifetimes for c-Si cell material are typically a few tens of microseconds, while lifetimes for GaAs cell material are much shorter, at around a few nanoseconds. While lifetimes in fabricated junctions can be different from the raw material, it is interesting to note that a typical c-Si lifetime is substantially longer than the pulse periods we considered, and the GaAs lifetime is shorter. Regardless, simulator photons are still able to effectively generate photocarriers in these two devices.

The discrepancies between the NIST and NREL measurements presented in Table I and Fig. 4 are significant and not random. The NIST values were consistently smaller than the NREL values, excluding the CIGS cells. The discrepancies have largely been accounted for by the handling, contacting, and illumination of the cells while at NIST. To further investigate what is anticipated to be a potentially small impact from the pulsed nature of the simulator will require the development of rigorous, quantitative measurement procedures, as well as refinements to the simulator itself. The comparison of types of simulators might best be accomplished by use of a single efficiency measurement setup in which only the light source is exchanged quickly and easily. At this time, the results indicate that for the four material systems studied, the supercontinuum simulator looks largely like the sun.

IV. Solar Simulator Focusing

The tight focusing of light sources for the microscopic excitation and study of solar cells has traditionally been done with lasers having single-mode beam quality. However, this excitation is not very sun-like because most lasers are spectrally very narrow. By contrast, the supercontinuum solar simulator offers both single-mode beam quality and a broad spectrum, which provides for more realistic characterization of solar cells.

Achieving a diffraction-limited focus puts stringent requirements on the quality of the optical beam impinging on the focusing element. Plane-wave illumination with a smooth Gaussian-like beam profile is preferred. For most solar simulators, this requirement is particularly challenging because of the broad spectral content and wide solid angle of the emission. While broadband light can often be efficiently coupled into and out of step-index multimode optical fiber, the resulting propagation and illumination are by nature spatially structured. However,

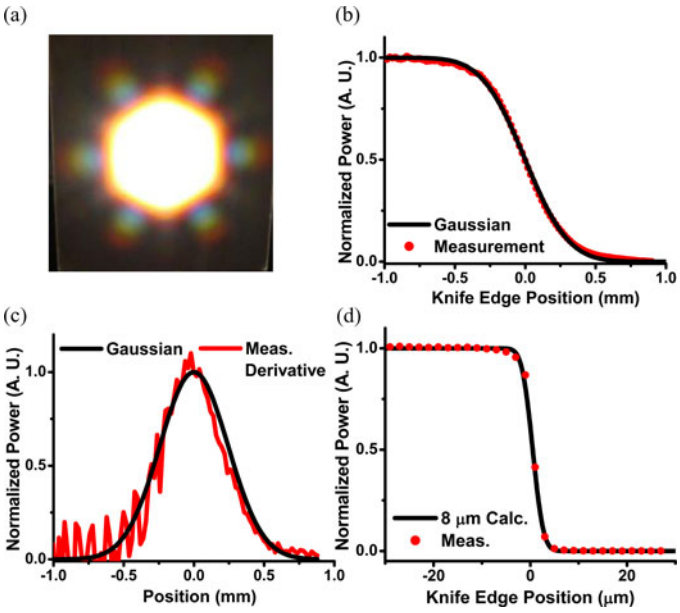

Fig. 5. (a) Projected light distribution emitted from the simulator output fiber. (b) Knife-edge measurement of the projected light. (c) Derivative of the measurement in (b) is compared with a Gaussian beam profile. (d) Knife-edge measurement of the focused spot.

photonic crystal fiber, as used to generate supercontinuum light, supports a broad bandwidth with flat dispersion and single-mode propagation. For the purposes of beam conditioning, we coupled the light exiting our spectral shaper into a 3-m-long photonic crystal fiber. While the coupling efficiency was greater than 100 times more lossy than coupling into a 200-μm multimode fiber, there was still more than enough light for applications with focused illumination.

Fig. 5(a) shows the projected spatial pattern of the light diverging from the end face of the photonic crystal fiber. The large central lobe represents broadband propagation of light within the 8-μm glass core of the fiber. Fig. 5(b) presents a knife-edge measurement [11] of the beam profile of the light a few millimeters from the end face. The red dots show the measured optical power that passed by the knife edge as it was slowly scanned across the beam. The optical power was measured with a thermal sensor to provide a flat response over the broad wavelength range of the simulator. The overlaid black curve of Fig. 5(b) is a least-squares fit to the measurement, assuming an idealized Gaussian beam profile, and shows excellent agreement. The red curve of Fig. 5(c) presents the derivative of the knife-edge measurement and has good average agreement with the black Gaussian profile. The intensity noise of the knife-edge measurement was dramatically enhanced by the point-to-point derivative operation and illustrates why it is better to curve-fit to the as–measured data. Surrounding the central lobe of Fig. 5(a) are six smaller lobes that represent propagation in the hexagonal array of air holes encircling the glass core. Considering that an otherwise saturated image was required to view them, the total power in the surrounding lobes is actually very small. The broadband single-mode propagation characteristics of the photonic crystal

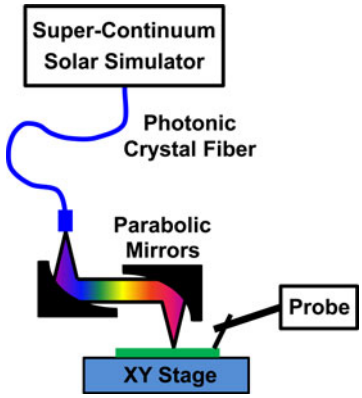

Fig. 6. Focusing of the solar simulator by use of parabolic mirrors with a motorized translation stage for raster-scanning image formation.

fiber are critical to achieving a high-quality Gaussian-like beam capable of being focused to a very small spot.

As shown in Fig. 6, the diverging light from the photonic crystal output fiber was collimated and focused by aluminum parabolic mirrors, having focal lengths of approximately 50 and 20 mm, respectively. We used the knife-edge technique to estimate the diameter of the focused spot to be about 8 μm, which, for a Gaussian beam, contains 86% of the beam power. The knife-edge measurement of the spot is presented in Fig. 5(d) and illustrates that the slope of the transmitted power through the central lobe (zero position) compares well to the prediction for an 8-μm Gaussian beam. A small deviation is apparent at the upper knee that may be caused by scattering of stray light. With refinements to the focusing optics, we anticipate that the spot size can be reduced to below 2 μm.

V. Full-Spectrum Optical-Beam-Induced Current Measurements

The short-circuit current induced by the focused simulator was spatially mapped across sample solar cells by use of a raster scanning system that translated the sample, as depicted in Fig. 6. In these FS-OBIC measurements, the irradiance of the focused spot was approximately equivalent to 160 suns. Fig. 7 shows the measured current map of an n–GaInP/p–GaAs heterojunction concentrator cell provided by the NREL. In this 500 μm $\times$ 500 μm image made with 10-μm translation steps, the depressed dark regions were caused by metallic grid lines on the cell, which shadowed the active material. The production of current from the active regions of the cell is indicated by the light-colored mesa structures and is about 1 μA. The highly uniform current map is consistent with the high efficiency of the device (measured to be 15.2% by the NREL) and the crystalline composition.

Fig. 8 presents the results of an FS-OBIC measurement on a CIGS thin-film solar cell, also from the NREL. The long trench feature was created by a grid line, and the induced current in the active regions was a little over 1 μA. The central crater was caused by a small scratch in the film intentionally created with a pin point and indicates the localized impact on the production of photocurrent. The active area of the cell shows a distinct

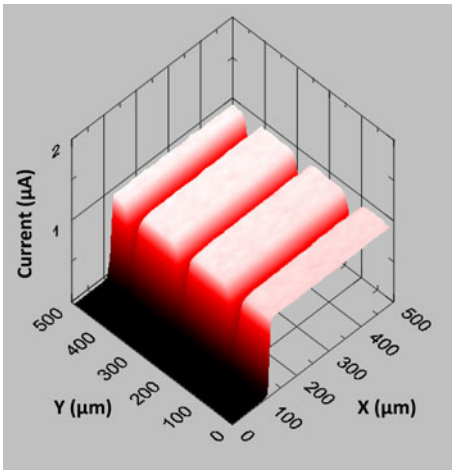

Fig. 7. Current map of a GaAs solar cell with grid lines.

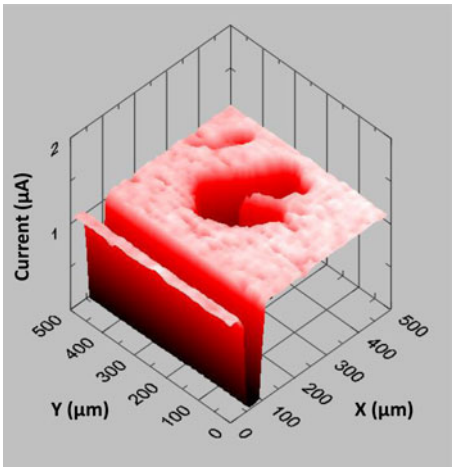

Fig. 8. Current map of a CIGS cell featuring a grid line, damage spot, and surface variations.

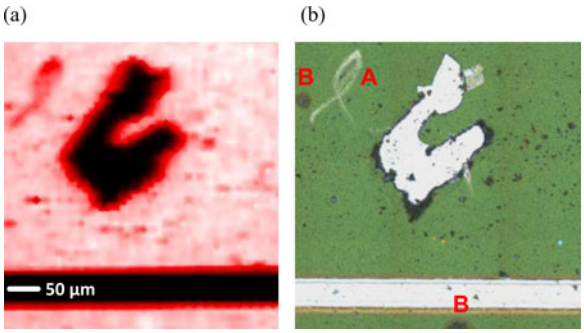

Fig. 9. (a) Top-view map of the CIGS cell image (see Fig. 8) with (b) an optical-microscopy image of the same region.

spatial variation or roughness. Typical of this CIGS material, grain structures of just a few micrometers in size are expected to be arranged in clusters of 10 μm or more.

Fig. 9(a) is a top view of Fig. 8, to enable side-by-side comparison with the optical microscopy image of the CIGS cell shown in Fig. 9(b). It is clear from the optical microscopy that the pin-point scratch caused complete removal of the thin film from the glass substrate. By contrast, the smaller ribbon-like feature in the upper left corner (labeled with "A") may constitute partial film damage, causing a slight reduction (darkening) in the current map. The small, dark, speckle features in Fig. 9(b) would appear to be film debris from creating the scratch. Some of their locations correlate with reductions in current. Two additional features of interest in Fig. 9(b) are a brown spot found to the left of the ribbon-like feature and another brown spot partially shown at the bottom center of the image (both labeled with "B"). In the upper left instance, the feature corresponds to a reduction in current (dark spot), while the lower one appears to generate increased current (white spot). A topographic image of this area of the cell indicated that these brown spots reside in the volume of the film, whereas the small speckle features rest on top. A better understanding of this sample may be obtained from measurements with higher spatial resolution.

We anticipate that a much smaller focused spot can be achieved through better utilization of our optical beam as well as better-quality optics. An approximate expression for the spot-size diameter of a focused Gaussian beam at wavelength λ by an objective with f-number *f#* is given by $2\lambda f\#$. The f-number of our focusing parabolic mirror was 0.5, which indicates that by use of the full diameter of the optic, we could achieve a spot equal to the wavelength of the light. This simple expression also indicates that the spot size has a linear wavelength dependence, which is of importance when considering a broadband light source. With our simulator, some of this dependence is offset by the spatial distribution of the simulator light [see Fig. 5(a)], in which the beam has more red content at the periphery. While further study is required, we anticipate that we can achieve a smaller spot that would enable the illumination of individual grains in thin films and nanostructures in engineered materials at a scale below 2 μm.

VI. Spectrum-Sliced and Multijunction Measurements

For the characterization of multijunctions with traditional light sources, the required optical excitation can become rather cumbersome, with multiple sources coincident from different angles with limited spectral selectivity. As the number of junctions to be tested in a device increases, so must the complexity of the optical excitation. To illustrate the ability of the supercontinuum simulator to create customized illumination for light biasing of multijunctions, we applied additional masks to slice the simulator spectrum into subbands. Fig. 10 presents measurements of four different spectra created for the excitation of individual layers in a four-junction solar cell.

To develop the multijunction measurement capabilities of the simulator, we characterized the partial currents generated by a single-junction cell from spectrally sliced illumination. Fig. 11 shows two sliced spectra created by the simulator, which we have colored and labeled as the blue and red spectra. The spectra were sliced at a wavelength of 720 nm so as to have nearly equal total power within the wavelength range shown. The external quantum efficiency (EQE) of a representative, single-junction, GaAs solar cell from the NREL, that is very similar to the device

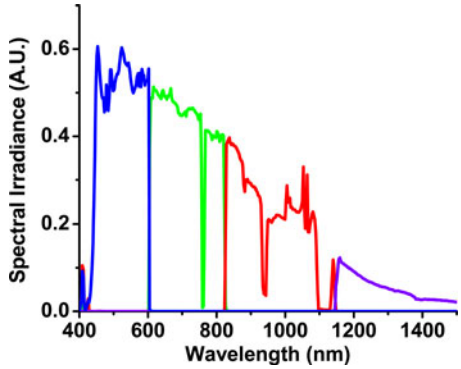

Fig. 10. Measured spectra are shown for the selective excitation of four multijunction cell layers.

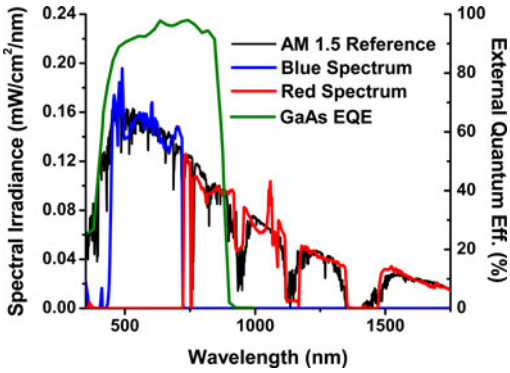

Fig. 11. Sliced spectra for inducing partial currents are shown with the EQE of a representative GaAs single-junction cell.

used throughout this work, is also shown in this figure [10]. While not the actual EQE of our device, the curve is a sufficient representation to estimate the measured partial currents when used in conjunction with the measured spectra.

Fig. 12(a) shows a full-spectrum OBIC measurement of the GaAs cell with a focused spot irradiance that was approximately equivalent to 50 suns. Fig. 12(b) and (c) shows the OBIC measurements for spectrally sliced blue and red illumination, respectively. The average currents measured in the middle of the active regions were 0.115 μA for the blue illumination and 0.055 μA for the red illumination. The sum of these currents agrees well with the 0.174-μA current measured for full-spectrum illumination in Fig. 12(a).

By using the curves of Fig. 11, we estimated that 73% of the total current should be produced from blue-light illumination, whereas the remaining 27% should be produced from red-light illumination. Because the EQE for this GaAs device rolls off substantially above 850 nm, more current is expected from blue illumination, despite the nearly equal optical powers delivered to the device. Comparing the currents of Fig. 12, we measured 68% of the current from blue illumination and 32% from red illumination. The agreement is quite good, keeping in mind that the actual EQE curve for the device was not available.

To demonstrate the measurement of individual junction characteristics in a tandem solar cell, biased spectra were created

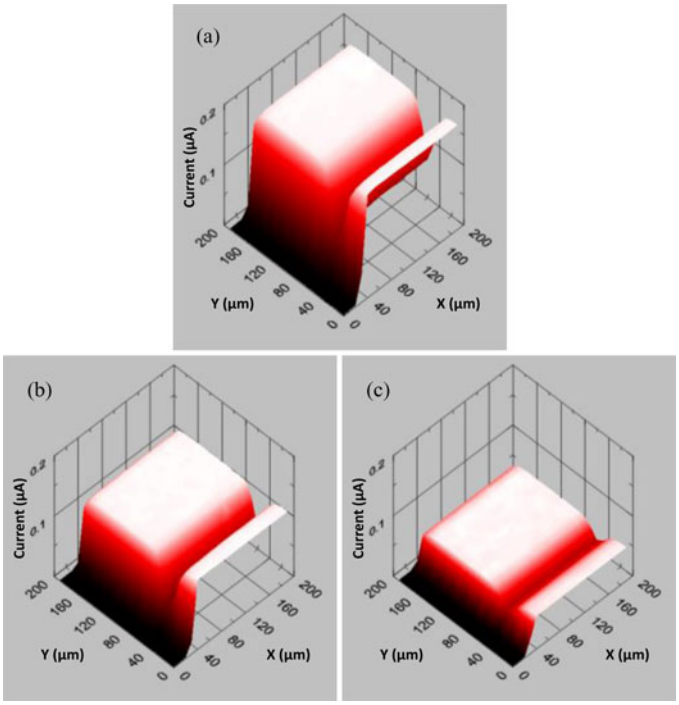

Fig. 12. Current maps for (a) full-spectrum illumination, (b) blue-light illumination, and (c) red-light illumination of a GaAs solar cell.

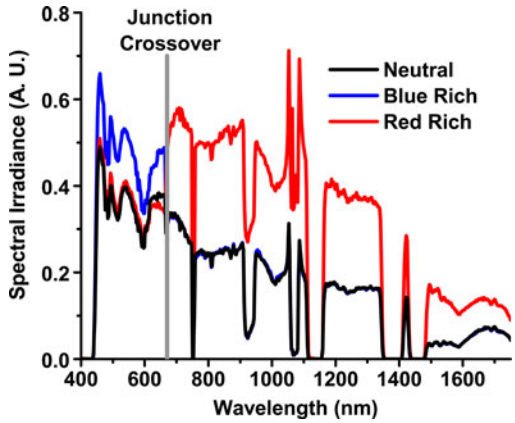

Fig. 13. Blue-rich and red-rich spectra used for the light-biasing of a series tandem cell are compared with a neutral spectrum. The bias light was split at a wavelength of 670 nm.

to implement the current-limiting technique described by Kurtz *et al*. [12]. The black curve of Fig. 13 shows the simulator spectrum for balanced neutral illumination of both junctions of a GaInP/GaAs tandem solar cell from the NREL. Plotted behind the black curve are blue-rich and red-rich spectra used to create bottom- (long wavelength) and top- (short wavelength) limited cell currents. In the respective unbiased wavelength regions for each curve, the spectra are closely matched and obscured by the neutral spectrum. As indicated by the gray vertical line, the biasing regions meet at a wavelength of 670 nm to correspond with the complementary EQE dependence of the two junctions. The amount of blue-rich and red-rich light bias could be varied continuously between the balanced neutral level and the

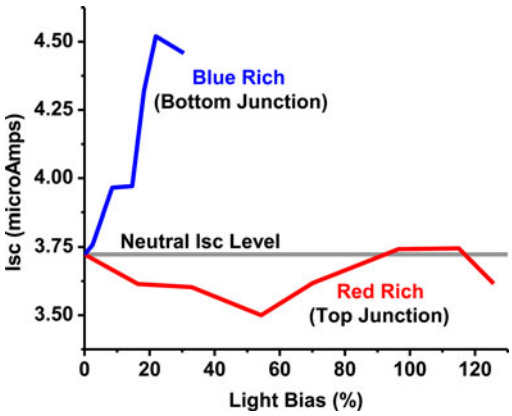

Fig. 14. Short-circuit currents for a GaInP/GaAs tandem cells are measured as a function of blue-rich and red-rich light bias. Current-limiting behavior is observed for the top junction.

maximum cases shown. The red-rich content could be more than doubled in optical power, whereas the blue-rich content could be increased by at most 30%.

Fig. 14 shows the measured short-circuit currents for the biased illumination of the GaInP/GaAs tandem cell across its full area of about 0.1 cm^2. Because of technical limitations at the time, the irradiance was limited to about 0.1 mW/cm^2, generating currents in the microamp range. The measured current for balanced illumination of both junctions resulting from the black spectral curve of Fig. 13 was 3.7 μA. In Fig. 14, this unbiased illumination scenario corresponds to the current shown for a light bias defined as 0%. For visual reference, this current level for neutral illumination has been extended across the plot with a horizontal gray line. As the red-light bias was increased up to 130%, the short-circuit current remained near the neutral level. This indicates that the tandem cell is top-junction limited, because substantial increases to the red-rich content result in no significant increases in cell current. Conversely, a 30% increase in the blue-rich content resulted in a 20% increase in cell current. This is consistent with the top junction producing more current, as allowed by the larger current-producing capacity of the bottom cell. With a limited amount of light bias available at this time, we were unable to extend the "blue-rich" curve far enough to measure the current limit for the bottom junction. Results provided by the NREL indicate that the bottom-junction current limit should be about 50% higher than the 3.7 μA measured for neutral illumination.

Our preliminary characterization of the current-limiting behavior of a tandem cell is promising. However, we anticipate that our results could be greatly improved through a number of technical refinements. For example, a more efficient spectral shaping and light collection process would have resulted in a 1-sun illumination condition and short-circuit currents in the milliamp range. Better spectral shaping efficiency would also increase the light-bias adjustment range, allowing the current limits for both junctions to be observed. It may be possible to supplement the missing spectral content below 450 nm with additional blue-light sources. Spatial studies of multijunctions would be possible by combining the focusing ability of our simulator with the generation of light-biasing spectra and would be of particular interest to uniformity studies of multijunction concentrator cells.

VII. Discussion and Conclusion

The results of this demonstration of a supercontinuum solar simulator are very promising and justify further development of this technology. An effort is underway to replace the static amplitude masks used in this study with a programmable spatial light modulator to dramatically improve functionality and performance. With improvements to the spectral shaping accuracy, the uncertainties associated with the comparisons made to the NREL cells could be dramatically reduced to provide more conclusive results. In the future, improvements in this technology may allow cell calibration measurements to be performed without applying spectral mismatch corrections required for traditional simulators [9]. Furthermore, the ability to rapidly and accurately tune the simulator spectrum would enable more realistic and complicated illumination of multijunctions that are not possible with traditional simulators. For example, cell efficiency could be studied in the laboratory as a function of diurnal variations.

A quantitative intercomparison of cell efficiencies is planned for the near future to provide rigorous validation of the supercontinuum simulator beyond this preliminary demonstration. In addition to simulator development, such work will require refinements to our handling, contacting, and illumination of reference solar cells.

We have shown that our novel solar simulator has the ability to be spectrally shaped with unprecedented accuracy and can generate cell efficiency performance from a variety of photovoltaic devices as if they had been illuminated by the sun. Focusing the full-spectrum simulator to a spot 8 μm in diameter allowed us to map and study current variations in FS–OBIC spatial images. The measurement conditions for FS–OBIC are more realistic than those performed with a narrowband laser and should be particularly advantageous for the characterization of multijunctions. We also demonstrated the spectrally selective generation of partial currents in a single-junction solar cell that was consistent with the device quantum efficiency. Finally, the simulator is capable of producing blue-rich and red-rich spectra to illustrate the current-limiting behavior of a tandem solar cell. Without added system complexity, the light biasing of three or more junctions could easily be accomplished within the single, collimated, or focused beam of our simulator.

Acknowledgment

The authors gratefully acknowledge A. Sanders of NIST for optical and topographic microscopy; D. Friedman, L. Mansfield, Q. Wang, and B. Nemeth of the NREL for providing sample cells and technical guidance; and O. Jonsson and PV Measurements, Inc. for the use of the xenon solar simulator.

REFERENCES

[1] T. Moriarty, J. Jablonski, and K. Emery, "Algorithm for building a simulator spectrum for NREL one-sun multi-source simulator," in *Proc. 38th Photovoltaic Spec. Conf.*, Austin, TX, USA, 2012, pp. 1291–1295.

[2] K. Emery, D. Myers, and S. Rummel, "Solar simulation—Problems and solutions," in *Proc. 20th Photovoltaic Spec. Conf.*, Las Vegas, NV, USA, 1988, pp. 1087–1091.

[3] Y. Tsuno, K. Kamisako, and K. Kurokawa, "New generation of PV module rating by LED solar simulator—A novel approach and its capabilities," in *Proc. 33rd Photovoltaic Spec. Conf.*, San Diego, CA, USA, 2008, pp. 1–5.

[4] B. H. Hamadani, J. Roller, B. Dougherty, and H. Yoon, "Fast and reliable spectral response measurements of PV cells using light emitting diodes," in *Proc. 39th Photovoltaic Spec. Conf.*, Tampa, FL, USA, 2013, pp. 0073–0075.

[5] J. M. Dudley, G. Genty, and S. Coen, "Supercontinuum generation in photonic crystal fiber," *Rev. Mod. Phys.*, vol. 78, no. 4, pp. 1135–1184, 2006.

[6] T. Binhammer, E. Rittweger, R. Ell, F. X. Kärtner, and U. Morgner, "Prism-based pulse shaper for octave spanning spectra," *Opt. Commun.*, vol. 41, no. 12, pp. 1552–1557, Dec. 2005.

[7] J. P. Rice, S. W. Brown, J. E. Neira, and R. R. Bousquet, "A hyperspectral image projector for hyperspectral imagers," *Proc. SPIE*, vol. 6565, p. 65650C, 2007.

[8] *Standard Tables for Reference Solar Spectral Irradiances: Direct Normal and Hemispherical on 37° Tilted Surfaces*, G173003, 2008 [Online]. Available: http://astm.org

[9] H. Field and K. Emery, "An uncertainty analysis of the spectral correction factor," in *Proc. 23rd Photovoltaic Spec. Conf.*, Louisville, KY, USA, 1993, pp. 1180–1187.

[10] S. R. Kurtz, J. M. Olson, and A. Kibbler, "High efficiency GaAs solar cells using GaInP2 window layers," in *Proc. 21st Photovoltaic Spec. Conf.*, Kissimmee, FL, USA, 1990, pp. 138–140.

[11] J. A. Arnaud, W. M. Hubbard, G. D. Mandeville, B. de la Clavière, E. A. Franke, and J. M. Franke, "Technique for fast measurement of Gaussian laser beam parameters," *Appl. Opt.*, vol. 10, no. 12, pp. 2775–2776, Dec. 1971.

[12] S. R. Kurtz, K. Emery, and J. M. Olson, "Methods for analysis of two-junction, two-terminal photovoltaic devices," in *Proc. World Conf. Photovoltaic Energy Convers.*, Waikoloa, HI, USA, 1994, pp. 1733–1737.

Authors' photographs and biographies not available at the time of publication.